Global Instantaneous Centimeter-Level Multi-constellation and Multi-frequency Precise Point Positioning with Cascading Ambiguity Resolution

Lizhong Qu(✉), Luping Wang, Haoyu Wang, Wei Jiang, and Yiwei Du

School of Geomatics and Urban Spatial Informatics, Engineering and Architecture, Beijing University of Civil, 1 Zhanlanguan Road, Beijing 100044, China
qulizhong@bucea.edu.cn

Abstract. With the progresses of Global Navigation Satellite System (GNSS), a number of satellites transmitting multi-frequency signals contribute precise point positioning (PPP). Global instantaneous or single-epoch centimeter-level PPP may be reached because global single-epoch narrow-lane (NL) ambiguity resolution (AR) may be possible with many wide-lane (WL) ambiguities being fixed instantaneously, which can improve the accuracy of the instant NL ambiguities. In this article, the cascading AR (CAR) method was extended to the GPS, Galileo, and BDS-3 all-frequency signals. The performance of instantaneous PPP was investigated with global public stations. The results showed that attributed to the additional frequency observations, the instant positioning accuracy improved substantially. On a global scale, the instant horizontal and up positioning accuracy improved from about 20 and 60 cm, respectively, for the dual-frequency PPP-CAR to about 6 and 20 cm, respectively, for the multi-frequency PPP-CARs. These results are quite encouraging for global autonomous driving cars because better positioning accuracy is expected once the multi-constellation and multi-frequency signals are integrated with inertial sensors.

Keywords: Instantaneous centimeter-level · Precise point positioning · Multi-constellation and multi-frequency · Cascading ambiguity resolution

1 Introduction

GNSS (Global Navigation Satellite System) precise positioning technology can provide users' absolute coordinates, which plays an indispensable role in automatic driving [1]. To achieve global instantaneous high-precision positioning, such as centimeter-level accuracy, single-epoch ambiguity resolution (AR) is a prerequisite [2]. GNSS short-baseline RTK technology eliminates atmosphere or instrumental errors, and single-epoch AR is easy [3]. However, with the increase in the distance between the rover and reference stations, the spatial correlation decreases, which results in the short operating distance (<10 km). Precise point positioning (PPP) employs a single GNSS receiver to realize

C. Yang and J. Xie (Eds.): CSNC 2024, LNEE 1094, pp. 269–278, 2024.
https://doi.org/10.1007/978-981-99-6944-9_23

high-precision positioning, which has wide application prospects in automatic driving. However, due to the slow variation of spatial geometry and the large noise of pseudo-range observations, it usually takes dozens of minutes to converge. Fortunately, for global instantaneous PPP, new opportunities are provided by multi-constellation and multi-frequency signals.

PPP AR usually contains two steps: wide-lane (WL) and narrow-lane (NL) AR. The WL ambiguities with long wavelengths are easily fixed instantaneously on a global scale, while the NL ambiguities with short wavelengths are difficult to be fixed instantaneously on a global scale because of the limited accuracy of global atmosphere corrections [4]. The PPP WL AR (PPP-WAR) model was proposed to improve the instant positioning accuracy by fixing a series of WL ambiguities instantaneously [5]. However, compared to the raw phase observation noise, because the noise of such WL ambiguity combinations was enlarged, only decimeter-level instant positioning on a global scale was achieved [6]. Fortunately, the PPP-WAR provides a new approach to achieve global fast NL AR. That is because many WL ambiguities being fixed instantaneously can improve the accuracy of the instant NL ambiguities even without atmosphere corrections [7–10].

However, studies on single-epoch NL AR were limited to regional scale. The distances among stations are much longer for the global reference network. Residual orbit or ionosphere errors may have a deleterious impact on single-epoch NL AR [4–11]. By fixing as many as possible WL ambiguities instantaneously, global single-epoch NL AR may be possible. In this article, the PPP-CAR method was extended to the GPS, Galileo, and BDS-3 all-frequency signals to investigate it.

2 Methodology

2.1 Observation Equations

The observation equations of the multi-constellation and multi-frequency code and phase measurements from receiver r to satellite s can be expressed as follows [12]:

$$\begin{cases} P^s_{r,i} = \rho^s_r + \tilde{t}^C_r - \tilde{t}^s + m^s_r T_r + g^C_{1i}\tilde{I}^s_{r,1} + IFB^s_{r,i} + \varepsilon_{P^s_{r,i}} \\ L^s_{r,i} = \rho^s_r + \tilde{t}^C_r - \tilde{t}^s + m^s_r T_r - g^C_{1i}\tilde{I}^s_{r,1} + \lambda^C_i \tilde{N}^s_{r,i} + \varepsilon_{L^s_{r,i}} \end{cases} \tag{1}$$

where C is the GNSS system; $i = 1, \cdots, n^C$, n^C denotes the total frequency number of system C; $P^s_{r,i}$ and $L^s_{r,i}$ denote the code and phase measurements at the *ith* frequency, respectively; ρ^s_r denotes the geometric distance; $\tilde{t}^C_r$ and $\tilde{t}^s_r$ denote the receiver and satellite clock errors, respectively; T_r is the zenith tropospheric delay (ZTD) with the mapping function m^s_r; $\tilde{I}^s_{r,1}$ is the slant ionospheric delay of the first frequency, $g^C_{1i} = \left(f^C_1/f^C_i\right)^2$, f^C_i is the value at the *ith* frequency; $\lambda^C_i = v/f^C_i$ is the wavelength, $\tilde{N}^s_{r,i}$ is the float ambiguity, v is the speed of the light in vacuum; $\varepsilon_{P^s_{r,i}}$ and $\varepsilon_{L^s_{r,i}}$ denote the code and phase observation noises, respectively, and the unmodeled multipath errors are assimilated into the observation noises. Specially, $IFB^s_{r,i}$ denotes the satellite- and receiver-dependent inter-frequency code bias (IFB) [13], when $i = 1$ or $i = 2$, $IFB^s_{r,i}$=0; when $i = 3, \cdots, n^C$, $IFB^s_{r,i} \neq 0$.

2.2 PPP Ambiguity Resolution

Once the UPD products are acquired as in [14], the PPP-CAR is implemented [15]. A series of single-difference (SD) between satellites WL ambiguities are formed and corrected with the SD WL UPDs:

$$\begin{cases} EN^{sp}_{wl,1n^C} = \tilde{N}^{sp}_{wl,1n^C} - \hat{d}^{sp}_{wl,1n^C} \\ \vdots \\ EN^{sp}_{wl,13} = \tilde{N}^{sp}_{wl,13} - \hat{d}^{sp}_{wl,13} \\ EN^{sp}_{wl,12} = \tilde{N}^{sp}_{wl,12} - \hat{d}^{sp}_{wl,12} \end{cases} \tag{2}$$

where $EN^{sp}_{wl,1n^C}, \cdots, EN^{sp}_{wl,13}$, and $EN^{sp}_{wl,12}$ are the SD WL ambiguities between satellite s and reference satellite p; $\hat{d}^{sp}_{wl,1n^C}, \cdots, \hat{d}^{s,jp}_{wl,13}$, and $\hat{d}^{s,jp}_{wl,12}$ are the SD WL UPDs; $EN^{sp}_{wl,1n^C}, \cdots, EN^{sp}_{wl,13}$, and $EN^{sp}_{wl,12}$ are corrected SD WL ambiguities. The corrected SD WL ambiguities with their covariance matrix are inserted into a partial AR (PAR) strategy [16] based on the least-squares ambiguity decorrelation adjustment (LAMBDA) method [17] to search the optimal integer solution subset $\widehat{N}^{sp}_{wl,1n^C}, \cdots, \widehat{N}^{sp}_{wl,13}$, and $\widehat{N}^{sp}_{wl,12}$. . They are taken as accurate range observations to update the information matrix and parameters in the square root information filter (SRIF).

Using the WL-fixed ambiguities, the SD IF combination ambiguities are formed to compute the SD NL ambiguities, which are corrected with the SD NL UPDs as follows:

$$\begin{cases} N^{sp}_{IF} \equiv (\sqrt{g^C_{12}} N^{sp}_1 - N^{sp}_2)/(\sqrt{g^C_{12}} - 1) = N^{sp}_{nl} + \widehat{N}^{sp}_{wl,12}/(\sqrt{g^C_{12}} - 1) \\ \hat{d}^{sp}_{nl} = (\sqrt{g^C_{12}} \hat{d}^{sp}_1 - \hat{d}^{sp}_2)/(\sqrt{g^C_{12}} - 1) \\ EN^{sp}_{nl} = N^{sp}_{IF} - \widehat{N}^{sp}_{wl,12}/(\sqrt{g^C_{12}} - 1) - \hat{d}^{sp}_{nl} \end{cases} \tag{3}$$

where, distinguish from (5), N^{sp}_1 and N^{sp}_2 denote the WL-fixed SD ambiguities; N^{sp}_{IF} denotes the WL-fixed SD IF combination ambiguities; $\widehat{N}^{sp}_{wl,12}$ is the fixed SD WL ambiguity; $\hat{d}^{sp}_1$ and $\hat{d}^{sp}_2$ are the SD UPDs; $\hat{d}^{sp}_{nl}$ is the SD NL UPD; EN^{sp}_{nl} is the SD NL ambiguity after correction. The SD NL ambiguities with their covariance matrix are inserted into the PAR strategy to search the optimal integer solution subset $\widehat{N}^{sp}_{nl}$. The new IF combination ambiguities are reconstructed to update the estimated parameters again.

3 Data Collection and Processing Strategy

A total of 154 stations from IGS (International GNSS Service) MGEX (Multi-GNSS Experiment) global reference network (ftp://igs.gnsswhu.cn/pub/gps/data/) were collected and shown in blue and red diamonds in Fig. 1. All stations are equipped with Septentrio receivers capable of receiving GPS, Galileo, and BDS-3 multi-frequency signals, which were used to estimate the UPD products following the strategy in [14, 15]. Sixty stations shown in red diamonds capable of receiving GPS, Galileo, and BDS-3 all-frequency signals were taken as rovers in the single-epoch PPP experiment.

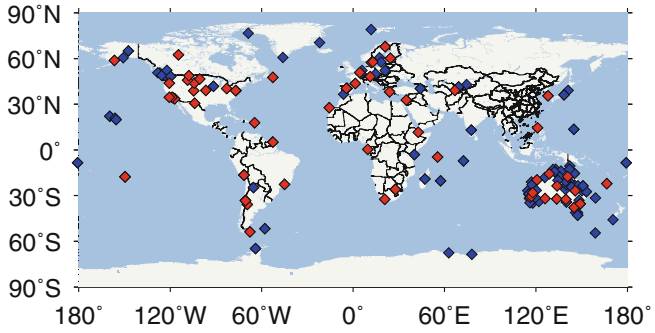

Fig. 1. Single-epoch PPP experiment station distribution.

The single-epoch dual-frequency (DF), triple-frequency (TF), quad-frequency (QF), and five-frequency (FF) float PPPs, PPP-WARs, and PPP-CARs were implemented. The processing strategy is shown in Table 1. To reduce the effects of the large propagation path errors on AR, the float ambiguities with average multi-epoch elevation below 20° were rejected from AR. To ensure the efficiency of searching and the validity of AR, in the partial AR (PAR) strategy, maximum 4 ambiguities could be removed, and minimum 5 ambiguities must be saved. The ratio value test was used to determine whether the PAR passed. The thresholds of the ratio value test used in WL and NL AR were 1.5 and 2.0, respectively. One week of data from March 12 to 18, 2022 (DOY 072–078) were processed. Only the daily data during GPS times 1:00–23:00 were used [18]. The ambiguities between neighboring epochs were reset. The single-epoch positioning results were compared to the GPS daily static solution with a 3D accuracy less than 1 cm. A total of 110880 epochs were used for the analysis of the results.

4 Results and Analysis

Figure 2 displays the instant positioning errors of single-epoch multi-frequency float PPPs, PPP-WARs, and PPP-CARs at station DGIJ. The multi-frequency float PPPs were the noisiest. Significant periodicity of the instant positioning error in the up component was found most likely due to the periodic multipaths of observations [19], which needed to be studied in the future work. With increasing frequencies, the amplitude decreased slightly, and thus, the instant positioning accuracies only had marginal improvements. The additional frequency observations had no effects on the multi-frequency float PPPs [20]. A submeter-level instant positioning accuracy was achieved due to the multi-constellation fusion. In contrast, the instant positioning accuracy of the single-constellation float PPP was at meter-level [12]. This demonstrated that the multi-constellation fusion improved the accuracy of the instant float ambiguities.

Though the DF PPP-WAR improved slightly than the DF float PPP, the periodicity was preserved in the DF PPP-WAR. Surprisingly, the amplitude decreased significantly for the multi-frequency PPP-WARs and the instant positioning accuracies improved significantly. This was because more WL ambiguities were fixed instantaneously. This also demonstrated that the accuracies of the instant float ambiguities of the TF, QF,

Table 1. The PPP processing strategy

Item	Model & Constraints
Observations	GPS: L1, L2, and L5 Galileo: E1, E5a, E6, E5, and E5b BDS-3: B1I, B3I, B2a, B1C, and B2b
Sampling	300 s
Elevation	7 °
Satellite orbit and clock products	Final precise orbit and clock error correction products from Wuhan University applied
Weight	2 m and 2 cm for the code and phase observations; elevation weighting strategy applied
Satellite and receiver antenna PCCs	igs14_2196.atx
Troposphere model	Saastamoinen model corrects the dry and wet components + Global Mapping Function (GMF)
Tidal and general relativistic effects	IERS 2010
Phase wind up	Corrected
GPS inter-frequency clock bias	Corrected
Parameter estimation	SRIF applied
Quality control	Detection, identification, and adaptation (DIA) method applied
Residual zenith troposphere wet delay	Piece-wise linear constant (PWC) with a process noise of 2 cm/$\sqrt{\text{h}}$ and a prior accuracy of 0.2 m
Slant ionospheric delays	Random-walking parameters with a loose process noise of 9 m/$\sqrt{\text{epoch}}$ and a prior accuracy of 90 m
Receiver clock error bias	Estimated as epoch-wise white noise parameters with a prior accuracy of 9,000 m
IFBs	Daily constant with a prior accuracy of 9,000 m
Station coordinates	Random-walk parameters with a loose process noise of 10 km/$\sqrt{\text{epoch}}$ and a prior accuracy of 100 km
Ambiguity	Noise parameters with a prior accuracy of 10,000 m

and FF PPP-WARs were further improved. In addition, the instant positioning errors in the horizontal component of the TF, QF, and FF PPP-WARs were very close and almost the same instant positioning accuracies of about 10 cm were achieved. This might have two reasons. On the one hand, the signals with similar frequencies had the similar contribution to the AR [5]. On the other hand, the frequency spaces [9] of the multi-frequency signals determined the magnified noises of the ambiguity combinations, which affected the positioning results [19]. However, with increasing frequencies, the instant positioning accuracies in the up component improved significantly.

Compared to the multi-frequency PPP-WARs, the instant positioning errors of the multi-frequency PPP-CARs decreased significantly and the instant positioning accuracy improved significantly attributed to NL AR, especially for the up component. Compared to the DF PPP-CAR, the TF, QF, and FF PPP-CARs had higher positioning accuracy, attributed to the higher reliability of NL AR being achieved. This was because the reliability of NL AR depended on the accuracy of instant NL ambiguities. According to (3), the NL ambiguities were from the float ambiguities. With the improvement of the accuracy of the instant float ambiguities, the accuracy of the instant NL ambiguities also improved. In addition, similar with the multi-frequency PPP-WARs, the instant positioning errors in the horizontal component of the TF, QF, and FF PPP-CARs were also very close, and more surprisingly, almost the same instant positioning accuracy of better than 10 cm was achieved. Meanwhile, with increasing frequencies, the instant positioning accuracy in the up component improved significantly.

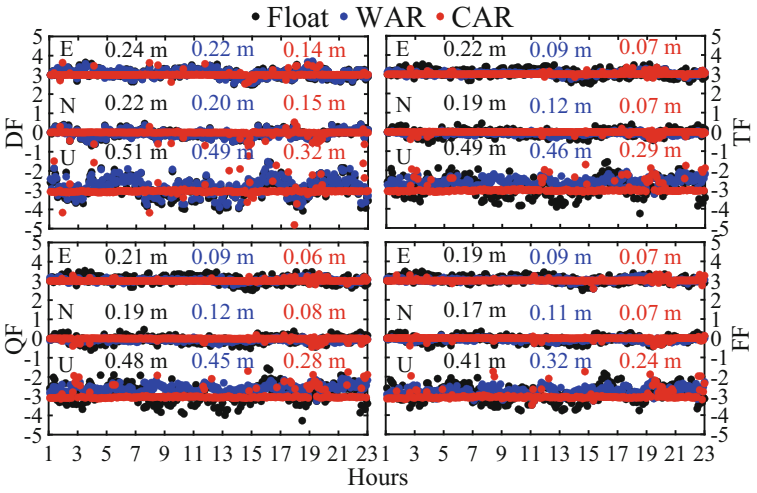

Fig. 2. Time series and daily RMS of the east (E), north (N), and up positioning errors (m) of single-epoch multi-frequency float PPPs, PPP-WARs, and PPP-CARs on March 15, 2022 (DOY 074) at station DJIG.

Figure 3 displays the distribution of the instant horizontal positioning errors of single-epoch multi-frequency float PPPs, PPP-WARs, and PPP-CARs of all rovers over one week. As the additional frequency observations had no effects on the multi-frequency float PPPs, the similar distribution was achieved for the multi-frequency float PPPs. With increasing frequencies, the percentages only had marginal improvements for the float PPPs. Compared to the DF float PPP, the distribution improved slightly for the DF PPP-WAR. However, compared to the multi-frequency float PPPs and the DF PPP-WAR, the distribution improved significantly for the TF, QF, and FF PPP-WARs with more WL ambiguities were fixed instantaneously. Attributed to the similar contribution from signals with the similar frequencies as well as the effects of the magnified observation noises caused from the frequency spaces, the percentages were very close for the TF,

QF, and FF PPP-WARs. Compared to the multi-frequency PPP-WARs, the distribution improved substantially for the multi-frequency PPP-CARs attributed to the NL AR. Compared to the DF PPP-CAR, the distribution improved substantially for the TF, QF, and FF PPP-CARs attributed to more reliable NL AR being achieved. Similar with the TF, QF, and FF PPP-WARs, the similar distribution was achieved for the TF, QF, and FF PPP-CARs, and with increasing frequencies, the percentages were slightly worse.

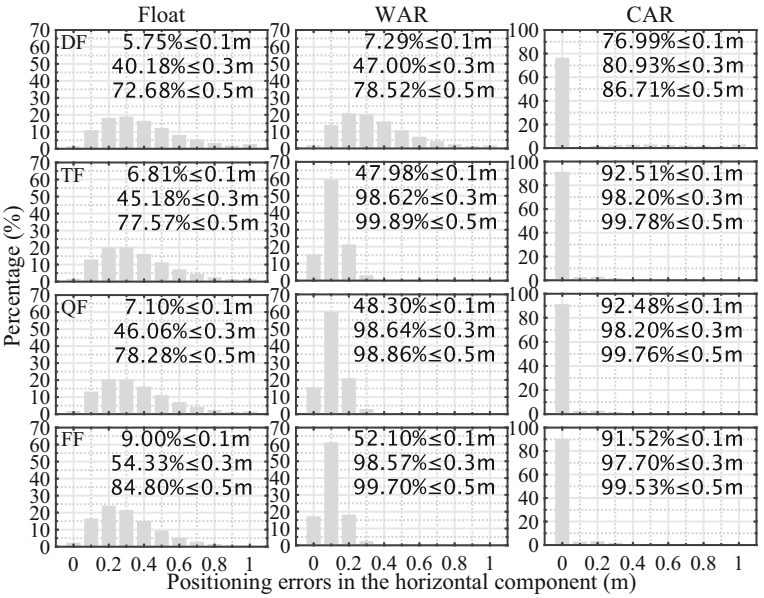

Fig. 3. Distribution of the instant horizontal positioning errors of single-epoch multi-frequency float PPPs, PPP-WARs, and PPP-CARs of all rovers over one week.

Figure 4 displays the distribution of the instant up positioning errors of single-epoch multi-frequency float PPPs, PPP-WARs, and PPP-CARs of all rovers over one week. Similar with Fig. 3, the similar distribution was achieved for the multi-frequency float PPPs. With increasing frequencies, the percentages only had marginal improvements for the float PPPs. Compared to the DF float PPP, the distribution improved slightly for the DF PPP-WAR. Compared to the TF and QF float PPPs and the DF PPP-WAR, the distribution of the instant positioning errors within 0.2 m was slightly worse for the TF and QF PPP-WARs. This was called the "ineffective WAR" [7]. Considering only less than 2% of instant positioning errors in the up component got worse, the phenomenon was not dominant. Except this, with increasing frequencies, the distribution improved significantly for the PPP-WARs and the FF PPP-WAR achieved the best among the multi-frequency PPP-WARs. This further demonstrated that with increasing frequencies, the contribution of fixing more WL ambiguities instantaneously to the instant positioning accuracy in the up component is more significant. Compared to the multi-frequency PPP-WARs, the distribution improved substantially for the multi-frequency PPP-CARs attributed to the NL AR. Compared to the DF PPP-CAR, the distribution improved

substantially for the TF, QF, and FF PPP-CARs. Meanwhile, with increasing frequencies, the distribution improved slightly for the PPP-CARs and the percentages also improved slightly, attributed to more reliable NL AR being achieved.

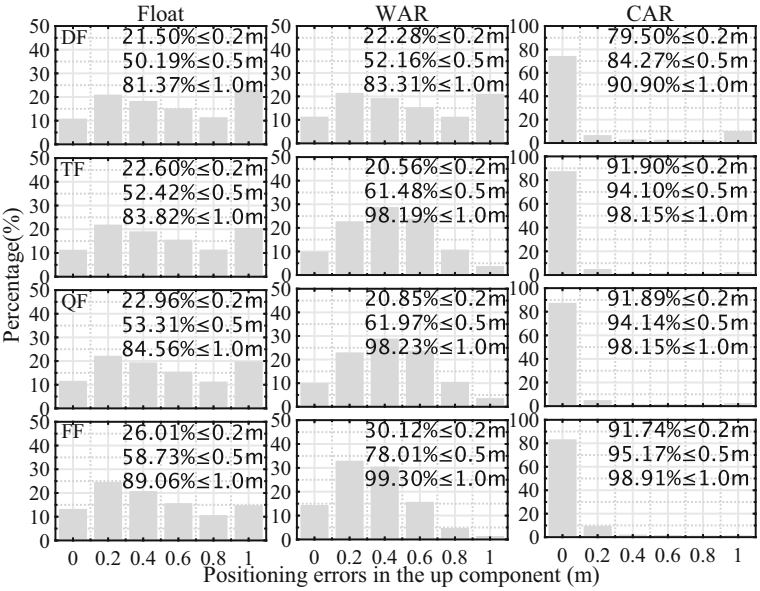

Fig. 4. Distribution of the instant up positioning errors of single-epoch multi-frequency float PPPs, PPP-WARs, and PPP-CARs of all rovers over one week.

The fixing rate was defined as the ratio of the number of epochs of the WL or NL AR passing the PAR test to the total number of epochs. According to Table 2, the instant positioning accuracies of the multi-frequency float PPPs were at the submeter-level. The instant positioning accuracies of the DF PPP-WAR and PPP-CAR were also at the submeter-level. The instant positioning accuracies of the TF, QF, and FF PPP-WARs improved substantially. Those in the horizontal component were close to 10 cm. The instant position accuracy of the TF, QF, and FF PPP-CARs also improved substantially. Those in the horizontal component reached the centimeter-level for the first time. The FRs of the WL ambiguities of the multi-frequency PPP-WARs were different with those of the multi-frequency PPP-CARs, which was related to the parameter constraint strategy. The FRs of NL ambiguities of the TF, QF, and FF PPP-CARs were slightly worse than that of the DF PPP-CAR, which demonstrated that more reliability of NL ambiguities was achieved.

Table 2. RMS (m) of the instant east, north and up positioning errors of single-epoch multi-frequency float PPPs, PPP-WARs, and PPP-CARs of all rovers over one week as well as the fixing rates (FRs) (%) of the WL and NL AR

PPP	Float PPP	PPP-WAR		PPP-CAR	
	RMS	RMS	WL FRs	RMS	WL/NL FRs
DF	0.31/0.35/0.78	0.28/0.32/0.74	99.94	0.22/0.24/0.57	99.92/99.90
TF	0.28/0.32/0.73	0.09/0.10/0.50	99.95	0.05/0.06/0.25	99.94/99.80
QF	0.28/0.31/0.72	0.09/0.10/0.50	99.86	0.06/0.06/0.24	99.83/99.71
FF	0.25/0.27/0.63	0.09/0.10/0.41	99.23	0.06/0.06/0.22	98.98/98.94

5 Conclusion

To investigate the global instantaneous PPP performance, we extended the uncombined PPP cascading WL/NL AR (CAR) method to the GPS, Galileo, and BDS-3 all-frequency signals. One week of data sampled at 300s of 60 global public stations evenly distributed from IGS MGEX were used in the single-epoch PPP experiment. The ambiguities were reset between neighboring epochs. A total of 110880 epochs were used for the analysis of the results. The results indicate that additional frequency observations only had a marginal improvement on the float PPPs. However, a submeter-level instant positioning accuracy were achieved due to the multi-constellation fusion, indicating that the multi-constellation fusion improved the accuracy of the instant float ambiguities to some extent. Although only decimeter-level instant positioning accuracies of the multi-frequency PPP-WARs were achieved due to the magnified noise of such WL ambiguities, the accuracies of the instant float ambiguities will be further improved. A centimeter-level horizontal instant positioning accuracy was achieved for the first time by the TF, QF, and FF PPP-CARs due to the contribution of the NL AR. However, compared with the DF PPP-CAR, the FRs of the NL ambiguities slightly decreased with increasing frequencies, which demonstrated that more reliable NL AR was obtained, because the accuracies of the instant NL ambiguities improved with the improvement of the accuracy of the instant float ambiguities.

Acknowledgments. This research was funded by National Natural Science Foundation of China (No. 42104026), Natural Science Foundation of Beijing Municipality (No. 4204094), General Research Project of Beijing Municipality Commission of Education (No. KM201910016007).

References

1. Geng J, Guo J, Chang H, Li X (2018) Toward Global Instantaneous Decimeter-level Positioning Using Tightly Coupled Multi-constellation and Multi-frequency GNSS. J Geod 93(7):977–991
2. Ge M, Gendt G, Rothacher M, Shi C, Liu J (2008) Resolution of GPS Carrier-phase Ambiguities in Precise Point Positioning (PPP) with Daily Observations. J Geod 82(7):389–399

3. Deng C, Tang W, Liu J, Shi C (2014) Reliable Single-epoch Ambiguity Resolution for Short Baselines Using Combined GPS/BeiDou System. GPS Solut 18(3):375–386
4. Gu S, Lou Y, Shi C, Liu J (2015) BeiDou Phase Bias Estimation and Its Application in Precise Point Positioning with Triple-frequency Observable. J Geod 89(10):979–992
5. Geng J, Guo J (2020) Beyond Three Frequencies: An Extendable Model for Single-epoch Decimeter-level Point Positioning by Exploiting Galileo and BeiDou-3 Signals. J Geod 94(1):1–15
6. Guo J, Xin S (2019) Toward Single-epoch 10-centimeter Precise Point Positioning using Galileo E1/E5a and E6 signals. In Proceedings of the 32nd International Technical Meeting of the Satellite Division of The Institute of Navigation (ION GNSS+ 2019). 2019: 2870–2887
7. Geng J, Guo J, Meng X, Gao K (2019) Speeding Up PPP Ambiguity Resolution Using Triple-frequency GPS/BeiDou/Galileo/QZSS Data. J Geod 94:1–15
8. Zhao Q, Pan S, Wang G, Wu B (2022) Multi-GNSS Fast Precise Point Positioning with Multi-frequency Uncombined Model and Cascading Ambiguity Resolution. Math Prob Eng
9. Laurichesse D, Banville S (2018) Innovation: Instantaneous Centimeter-level Multi-frequency Precise Point Positioning. GPS World July 4. 2018. Available online: https://www.gpsworld.com/innovation-instantaneous-centimeter-level-multi-frequency-precise-point-positioning/
10. Tao J, Chen G, Guo J, Zhang Q, Liu S, Zhao Q (2022) Toward BDS/Galileo/GPS/QZSS Triple-frequency PPP Instantaneous Integer Ambiguity Resolutions without Atmosphere Corrections. GPS Solut 26(4):1–14
11. Gu S, Lou Y, Shi C, Liu J (2015) BeiDou Phase Bias Estimation and Its Application in Precise Point Positioning with Triple-frequency Observable. J Geod 979–992
12. Qu L, Zhang P, Jing C, Du M, Wang J, Zhao Q (2021) Li J (2021) Estimating the Fractional Cycle Biases for GPS Triple-frequency Precise Point Positioning with Ambiguity Resolution Based on IGS Ultra-rapid Predicted Orbits. Remote Sens 13(16):3164
13. Qu L et al (2019) Precise Point Positioning Ambiguity Resolution by Integrating BDS-3e into BDS-2 and GPS. GPS Solut 23:63
14. Qu L, Wang L, Acharya TD, Du Y, Wang H, Jiang W (2023) Global single-epoch narrow-lane ambiguity resolution with multi-constellation and multi-frequency precise point positioning. GPS Solut 27(1):1–11
15. Qu L, Du Y, Wang H, Jiang W, Wang L (2023) Multi-constellation and multi-frequency precise point positioning with fast ambiguity resolution on a global scale. Measurement 112642
16. Wang J, Feng Y (2012) Reliability of Partial Ambiguity Fixing with Multiple GNSS Constellations. J Geod 87:1–14
17. Teunissen PJG (1995) The Least-squares Ambiguity Decorrelation Adjustment: A Method for Fast GPS Integer Ambiguity Estimation. J Geod 70:65–82
18. Zhao Q et al (2022) Precise Orbit Determination for BDS Satellites. Satellite Navi 3(1):25
19. Zhang Z (2021) Code and Phase Multipath Mitigation by Using the Observation-domain Parameterization and Its Application in Five-frequency GNSS Ambiguity Resolution. GPS Solut 25:144
20. Guo J, Geng J, Wang C (2021) Impact of The Third Frequency GNSS Pseudorange and Carrier Phase Observations on Rapid PPP Convergences. GPS Solut 25(2):1–12